Storage dynamics, hydrological connectivity and flux ages in a karst catchment: conceptual modelling using stable isotopes

Zhicai Zhang[1,2,4], Xi Chen[3,1], Chris Soulsby[2], Qinbo Cheng[1,4]

[1]State Key Laboratory of Hydrology-Water Resources and Hydraulic Engineering, Hohai University, Nanjing 210098, China

5 [2]School of Geosciences, University of Aberdeen, Aberdeen AB24 3UF, United Kingdom

[3]Institute of Surface-Earth System Science, Tianjin University, Tianjin China

[4]College of hydrology and water resources, Hohai University, Nanjing 210098, China

Correspondence to: Zhicai Zhang (zhangzhicai_0@hhu.edu.cn)

Abstract: We integrated unique high temporal resolution hydrometric and isotope data to calibrate a catchment-scale

10   conceptual flow-tracer model representing the two main landscape units of hillslopes, and depressions (with fast and slow flow systems) for cock-pit karst terrain. The model could track hourly water and isotope fluxes through each landscape unit, and we could estimate the associated storage and water age dynamics. This inferred that the fast flow reservoir in the depression had the smallest storage, the hillslope unit was intermediate, and the slow flow reservoir had the largest. The estimated mean ages of the hillslope unit, fast and slow flow reservoirs were 137, 326 and 493 days, respectively. Marked seasonal variability

15   in hydroclimate conditions and associated water storage dynamics were the main drivers of non-stationary hydrological connectivity between the hillslope and depression. Meanwhile, the hydrological connectivity between the slow and fast slow reservoirs had reversible directionality, which was determined by the hydraulic head within each medium. Sinkholes can make an important hydrological connectivity between surface water and underground stream flow in the fast reservoir after heavy rain. New water recharges the underground stream via sinkholes, introducing younger water in the underground stream flow.

20   **1 Introduction**

Karst aquifers are characterized by complex heterogeneous and anisotropic hydrogeological conditions which are very different to most other geological formations (Bakalowicz, 2005; Ford and Williams, 2013). The hydrological function of the critical zone in cockpit karst landscapes is consequently dominated by the strong influence of this unique geomorphology and the structure of carbonate rocks. Subsurface drainage networks in karst aquifers form mixed-flow systems that integrate flow

25   paths with markedly different flow velocities, ranging from low velocities in the matrix and small fractures, to very high velocities in large fractures and conduits (which often form subterranean channel networks), with associated transitions between states of laminar and turbulent flow (White, 2007; Worthington, 2009).

Due to the high spatial variability of the hydrodynamic properties of the karst critical zone, karst hydrological models are often conceptual, and are generally lumped at the catchment scale (e.g. Rimmer and Salingar, 2006; Fleury et al., 2007; Jukic and

30   Denic-Jukic, 2009; Tritz et al., 2011, Hartmann et al., 2013; Ladouche et al., 2014). Such lumped approaches, mostly based

on linear or nonlinear relationships between storage and discharge, conceptualize the physical processes at the scale of the whole karst system. However, semi-distributed lumped models need to have hydrogeological units adequately represented, in order to relate water flow in different landscape units and model parameters that have physically meaningful concepts. In order to avoid over-parameterisation (Perrin et al., 2001; Beven, 2006), many lumped models use rather simple model structures and

35   focus on key karst processes deemed to be dominant at particular study sites. Consequently, appropriate conceptualization of the structure and function of karst aquifers at the catchment scale is a central challenge for successful lumped modelling. Three main types of porosities – (a) micropores, (b) small fractures, and (c) large fractures and conduits – can be intuitively identified in karst systems. However, these are usually differentiated into two major categories of the matrix flow and conduit flow in conceptual models. Accordingly, the behavior of karst spring hydrographs, is often conceptualized as a two-reservoir model

40   to represent the dual flow system of the karst aquifer: A low permeability "slow flow" reservoir captures the function of fractured matrix blocks of the aquifer, whilst a highly permeable "fast flow" reservoir represents the larger karst conduits (Rimmer and Hartmann, 2012; Hartmann et al, 2014; Zhang et al, 2017). Based on such a strategy, structures such as soil/epikarst, vadose zone or groundwater system are usually sub-divided into different reservoirs to simulate the hydrological response of the karst aquifer at the catchment scale. However, this kind of approach cannot disaggregate water storage and

45   flux dynamics within different landscape units, and may be inadequate for modelling when understanding known spatial differences in hydrogeological structure is important in terms of provisioning water supplies and understanding water quality issues (Fu et al, 2016; Zhang et al, 2013). In addition, changing hydrological connectivity between different landscape units (e.g. hillslopes and depressions) is often a key control on the non-linearity of the flow responses of karst systems, though this is usually not explicitly represented in most conceptual models.

50   The utility of using tracers in karst hydrology is well-established and has given insights into advection-dispersion processes, physical exchange between conduits and smaller fractures/matrix, as well as identifying relevant contaminant transport parameters (e.g. Field and Pinsky, 2000; Goldscheider et al, 2008; Kübeck et al, 2013 Kogovsek and Petric, 2014). More generally, integration of tracers into rainfall-runoff models is becoming more common in hydrology and shows promise as such tracer-aided models can provide useful learning tools in hypothesis testing regarding water and solute transport (Birkel

55   and Soulsby, 2015a). Indeed, McDonnell and Beven (2014) have argued that such models provide a basis for ensuring that both the celerity (i.e. the speed) of the hydrological response can be captured, along with the velocity of individual water particles (i.e. the travel times) can be captured. Moreover, they identify this as one of the fundamental challenges for contemporary hydrological modelling.

In many studies, such tracer aided models have helped resolve the celerity-velocity dichotomy (Kirchner, 2003). Such

60   integration has helped to understand the functional influence of heterogeneity in catchment landscapes; the importance of hydrological connectivity between different landscape units and the mixing processes that regulate solute transport and control

water ages, as well as generating runoff responses (Jencso et al., 2010; Tetzlaff et al., 2014; Soulsby et al., 2015). Whilst tracer-aided models that conceptualize the transport of tracers through the karst systems via advection-dispersion, mixing, flow partitioning through different conduits, and exchange of tracer with the matrix have been widely used (Morales et al, 2010;

65   Charlier et al., 2012; Mudarra et al, 2014; Dewaide et al, 2016); recent modeling advances that use natural tracers, such as stable isotopes, to track water storage, flux and age dynamics have seen limited application in karst environments. Yet estimating transit times, water ages and storage dynamics with such models can provide useful metrics to characterize the karst critical zone. Additionally, incorporating isotope tracers into such models facilitates multi-objective calibration, which provides the opportunity to improve the rigor of model evaluation, constrain parameter sets and potentially reduce uncertainty

70   (Birkel et al, 2015b; Ala-Aho et al, 2017a).

Hydrological connectivity, which has been simply defined as the transfer of water from one part of the landscape to another (McGuire and McDonnell, 2010; Golden et al, 2014; Soulsby et al., 2015), relates to the flux of water across the landscape in different flow paths and in so doing is affected by and affects different landscape characteristics. Hydrologic connectivity is often highly dynamic in that connections/disconnections change seasonally and episodically during rainfall events. Even

75   though a connection may occur between two parts of the landscape, it does not necessarily suggest that water travels between those regions over the time scale of an event (McGuire and McDonnell, 2010). Connectivity is particularly relevant in karst areas as the complex subsurface hydrogeological conditions leads to frequent changes of hydrological connectivity. The system changes through periods of connection and disconnection to create dynamic feedbacks, which in turn will influence system function. Thus, understanding hydrological connectivity changes can provide key insights into the dominant processes

80   governing water and solute fluxes (Lexartza-Artza and Wainwright, 2009).

A major focus for hydrological research into karst critical zone function within the South West China karst region is the 1.25km^2 Chenqi catchment in Guizhou province. This catchment has typical cockpit karst landscape and associated karst critical zone architecture (Zhang et al., 2017). The specific aims of the paper are: (a) to simulate flow, storage, and tracer dynamics within different landscape units using a conceptual flow-tracer model; (b) to assess the nature of hydrological

85   connectivity between different landscape units and its controlling factors and; (c) to estimate the effects of time-varying hydrological connectivity in karstic landscapes on non-stationary water ages.

2 Study catchment and data

2.1 Study catchment

The study catchment of Chenqi, with an area of 1.25km^2, is located at the Puding Karst Ecohydrological Observation Station

90   in Guizhou Province of southwest China (Fig. 1). It is a typical cockpit karst landscape, with surrounding conical hills separated by star shaped valleys. The catchment, which is drained by a single underground channel/conduit, can be divided into two

units: depression areas with low elevation (<1340m) and steeper hillslopes with high elevation ranging from 1340~1500m. The spatial extent of the depression and hillslopes is 0.37 and 0.88 km², respectively.

Geological strata in the basin include dolostone, thick and thin limestone, marlite and Quaternary soil profiles (see cross-

95   sections of A-A' and B-B' in Fig 1). Limestone formations dominate the higher elevation areas with 150-200 m thickness, which lie above an impervious marlite formation. Therefore, precipitation recharging can be perched on the impervious marlite layers that discharges at the lower areas (mostly as hillslope springs). In the hillslopes, Quaternary soils are thin (less than 30cm) and irregularly developed on carbonate rocks. The outcrops of carbonate rocks cover 10-30% of the hillslope area. In the depression, soils are thick (> 2m deep). Dominant vegetation ranges from deciduous broad-leaved forest on the upper and

100   middle parts of the steep hillslopes to corn and rice paddy in the lower gentle foot slopes and depressions, where soils are also thicker. The paddy fields are often flooded for the heavy rainfall in summer. Additionally, there are three sinkholes outcropped in the depression where the surface and subsurface runoff can be directly drained into underground channel for the heavy rainfall events.

The catchment is located in a region with a subtropical wet monsoon climate with mean annual temperature of 20.1℃, highest in July and lowest in January. Annual mean precipitation is 1140 mm, almost all falling in a distinct wet season from May to

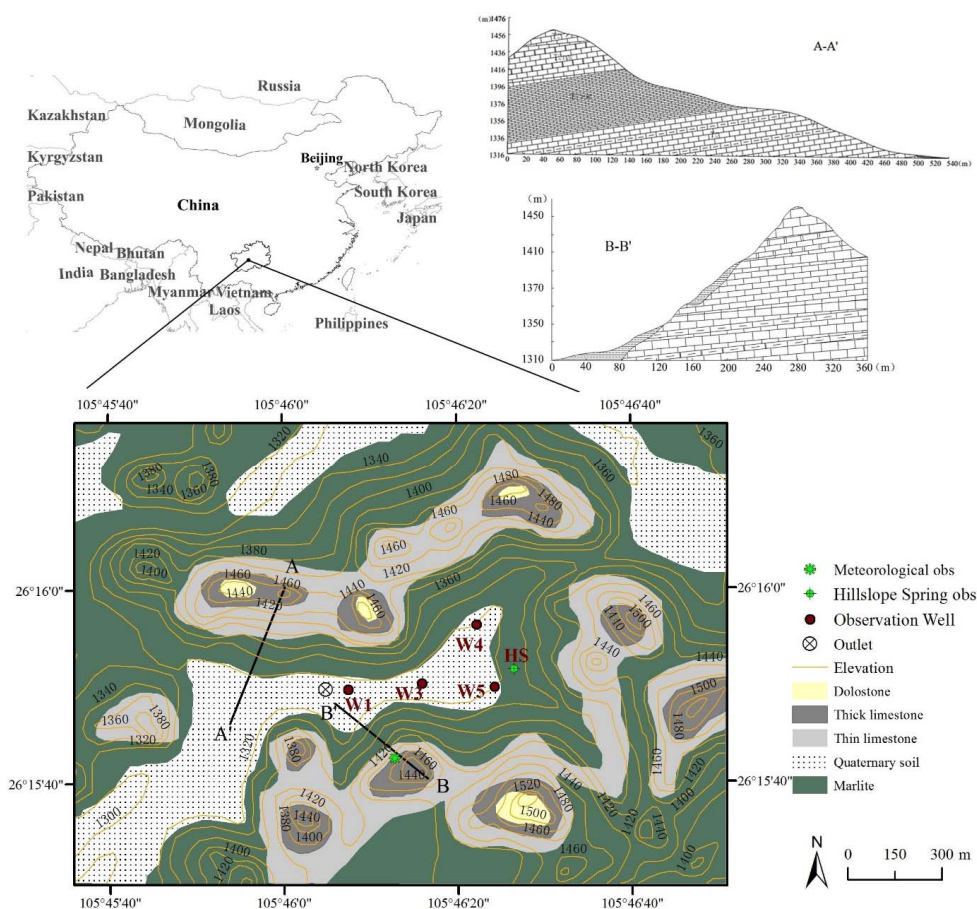105   September and a dry season from October to April. Average monthly humidity is high, ranging from 74% to 78%.

Hydrology and
Earth System
Sciences
Discussions

Figure 1 Map of location, geology, geomorphology and hydrological monitoring locations in the Chenqi catchment

2.2 Hydrometric and isotopic data

110   In Chenqi catchment, the discharge of a hillslope spring (HS) located at the foot of the eastern steep hillslope, and the

underground channel at the catchment outlet were measured with v-notch weirs (Figure 1). Their water levels were

automatically recorded by HOBO U20 water level logger (Onset Corporation, USA) with a time interval of 15 minutes.

Additionally, an automatic weather station was established on the upper hillslope to record precipitation, air temperature, wind,

radiation, air humidity and pressure. The data collection ran from 28 July 2016 to 30 October 2017. Statistical characteristics

115   of discharges at the spring and outlet are shown in Table 1.

Table 1 Statistical summary of flow discharge for hillslope spring (HS) and catchment outlet (m3/s)

Obs	Min	Max	Range	Mean	Cv
Outlet	0	0.15	0.15	4.7×10^{-3}	2.83
HS	0	1.4×10^{-3}	1.4×10^{-3}	8.5×10^{-5}	1.73

Hydrology and
Earth System
Sciences
Discussions

For isotope analysis, precipitation, the hillslope spring and catchment outlet flows were intensively sampled during eight

rainfall events in the wet season (May to October 2017) using an autosampler set to hourly intervals (form 12 June to 14

120   August 2017). Groundwater in the low elevation depressions was also sampled from four wells (Figure 1), with depth below

the ground surface ranging from 13 to 35m, during four rainfall events. The well screening was installed over the whole depth

for each of the wells to reflect local flow exchanges at various depths in the karst. In each event, groundwater samples were

collected before, during and after rainfall at each well from multiple depths.

All water samples were collected by 5 ml glass vials. The stable isotope composition of δ^2H (δD) and $\delta^{18}O$ ratios were

125   determined using a MAT 253 laser isotope analyser (the instrument precision ±0.5‰ for δ^2H and ±0.1‰ for $\delta^{18}O$). Isotope

ratios are reported in the d-notation using the Vienna Standard Mean Ocean Water standards. Statistical characteristics of

isotope signature are summarized in Table 2.

Table 2 Statistical summary of isotope data for rainfall, hillslope spring (HS), catchment outlet and depression wells

Obs	δD (‰)					$\delta^{18}O$ (‰)					lc-excess
	Max	Min	Range	Cv	Mean	Max	Min	Range	Cv	Mean	
Rainfall	-17.9	-120.2	102.3	0.3	-73.2	0	-16.4	16.4	0.29	-9.9	-0.59
Outlet	-46.9	-73.1	26.2	0.06	-61.9	-5.1	-10.6	5.5	0.09	-8.7	1.13
HS	-51.8	-77	25.2	0.04	-64.3	-5.9	-10.8	4.9	0.06	-9.3	2.91
W1	-50.7	-65.7	15	0.03	-60.8	-6.3	-9.6	3.3	0.05	-8.7	1.72
W3	-56.1	-73.6	17.5	0.06	-62.4	-7.4	-10	2.6	0.06	-8.7	0.66
W4	-55	-70.2	15.2	0.07	-62.5	-7.9	-10.1	2.2	0.07	-8.9	2.37
W5	-55.7	-67.5	11.8	0.03	-58.7	-7.9	-10.1	2.2	0.04	-8.5	2.39

3 Methodology

130   **3.1 Modeling approaches**

The model used in the study was developed in previous work that used tracer data in addition to stream discharge to constrain

the model structure, improve parameterization, and aid calibration (Zhang et al., 2017). The reader is referred to the original

paper for full details. Briefly, this model was developed to simulate the catchment-scale water and solute transport in the dual

flow system of the karst critical zone at daily time-steps. Consequently, it did not spatially disaggregate differences in flow

135   and tracer dynamics in different landscape units. Here we improved the model structure by separately conceptualizing the

dominant hillslope and depression landscape units (Figure 2), and then use the hourly discharge and isotope time series to

drive the modeling process. As Figure 2 shows, in this application, the Chenqi catchment was sub-divided into two spatially

distinct units to represent the hillslope and depression and precipitation was partitioned between them. Subsequently, the

depression unit was conceptualized into two flow systems, represented by "fast" and "slow" flow reservoirs which could also

140   exchange water. In contrast, the hillslope unit was conceptualized as just one reservoir, because of dominance of the thin

soil/epikarst on water flow and lack of major aquifer influence in the steep topography (Zhang et al., 2013).
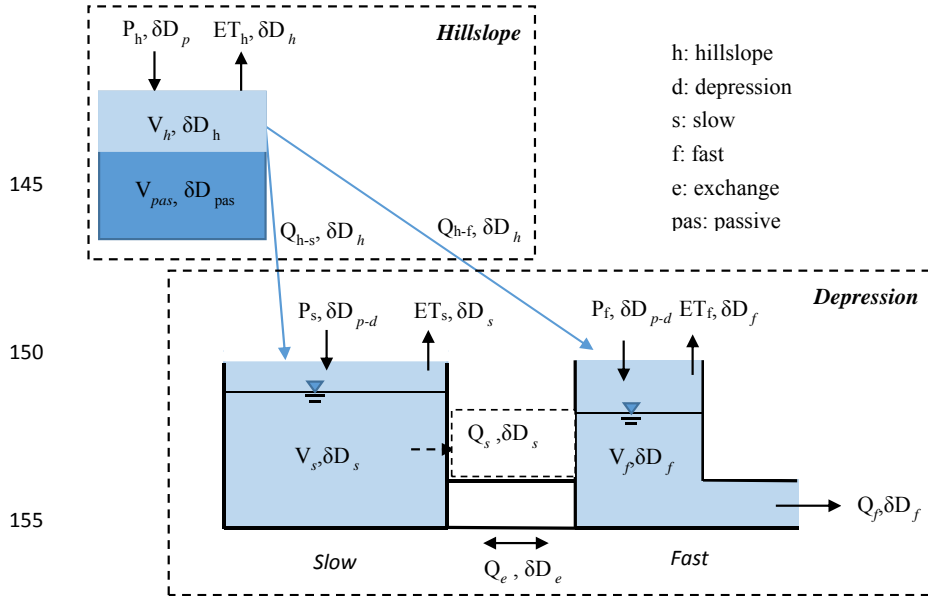
Figure 2 Structure of the coupled flow tracer model (modified from Zhang et al., 2017). Calculation of variables and storages are presented in Appendix A.

3.1.1 Hydrological simulation

The water balance in each of three reservoirs (hillslope unit, fast flow and slow flow reservoirs in depression) in the catchment are expressed as follows:

$$\frac{dV_h}{dt} = P_h - ET_h - Q_{h-s} - Q_{h-f} \tag{1}$$

$$\frac{dV_s}{dt} = P_s - ET_s + Q_{h-s} - Q_e \tag{2}$$

$$\frac{dV_f}{dt} = P_f - ET_f + Q_{h-f} + Q_e - Q_f \tag{3}$$

where P is rainfall (m3 hour-1), ET is evapotranspiration (m^3 hour^{-1}), Q is flow discharge (m^{3}hour^{-1}) and V is storage (m^3); subscripts of h, s and f represent the hillslope, slow and fast flow reservoirs, respectively, the subscripts of h-s and h-f represent from hillslope reservoir to slow and fast flow reservoirs, respectively, and subscript of e represents flow exchange between fast and slow reservoirs. The hydrological connection and flow discharge routing for the dual flow system in the depression was derived by Zhang et al. (2017). Here, we further include the hydrological connectivity of the hillslope flow discharging into the depression reservoirs ($Q_{h-s} \ and \ Q_{h-f}$ in Eqs. (1)~(3)).

3.1.2 Simulation of isotope ratios and estimation of water ages

The model tracks and simulates the isotope ratios for each reservoir separately, in which the isotope ratios can be complete or

175   partial mixed. Experimental evidence suggests that the common complete mixing assumption is overly-simplistic, in particular

for systems with pronounced switches between rapid shallow subsurface (e.g. macropores) or overland flow on the one hand

and slow matrix flow on the other hand (Van Schaik et al., 2008; Legout et al., 2009). Since the depression unit was divided

into the connected fast and slow reservoirs, a complete mixing of the isotope ratios is assumed for either reservoir. The hillslope

unit was conceptualized as a single reservoir in the new model, and complete mixing was too simplified. Hence, a partial

180   mixing was assumed for the hillslope (e.g. the upper active storage V_h mixing with the lower passive storage V_{pas} in Fig 2).

In the depression unit, the isotope mass balance in the slow and fast flow reservoirs can be expressed as:

$$\frac{di_s(V_s)}{dt} = i_{p-d}P_s - i_sET_s + i_hQ_{h-s} - i_sQ_e \tag{4}$$

$$\frac{di_f(V_f)}{dt} = i_{p-d}P_f - i_fET_f + i_hQ_{h-f} + i_sQ_e - i_fQ_f \tag{5}$$

where i is the δ^2H signature of the storage components (‰), the subscript of p-d represents rainfall infiltration in depression

185   unit.

In the hillslope unit, only a part of the mobile water contributing to hillslope flow is mixed with water in V_{pas} according to

$$\frac{di_h(V_h)}{dt} = i_pV_{p\_h} + i_{pas}V_{p\_pas} - i_hET_h - i_hQ_{h-s} - i_hQ_{h-f} + i_{pas}V_{pas\_in} - i_hV_{pas\_in} \tag{6}$$

$$\frac{di_{pas}(V_{pas})}{dt} = i_pV_{p\_pas} - i_{pas}V_{p\_pas} + i_hV_{pas\_in} - i_{pas}V_{pas\_in} \tag{7}$$

The additional volumes V_{pas} (m³) is the storage of passive reservoir in hillslope which is available to determine isotope storage,

190   mixing, and transport in a way that does not affect the dynamics of water flux volumes. V_{pas_in} (m³) is water volume from the

active store to the passive store. V_{p_h} and V_{p_pas} (m³) are the volume of rainfall into active and passive stores, respectively.

To further quantify how catchment functioning affects water partitioning, storage and mixing, water ages are also tracked in

the model. For water age estimation in the fast and slow flow reservoirs in the depression unit, complete mixing of the inputs

is assumed and ages tracked according to determine the dynamic storage volumes on an hourly time step:

195   $$\frac{dAge_s(V_s)}{dt} = Age_pP_s - Age_sET_s + Age_hQ_{h-s} - Age_sQ_e \tag{8}$$

$$\frac{dAge_f(V_f)}{dt} = Age_pP_f - Age_fET_f + Age_hQ_{h-f} + Age_sQ_e - Age_fQ_f \tag{9}$$

where Age is the water age.

For the age of the hillslope reservoir, the partial mixing is used:

$$\frac{dAge_h(V_h)}{dt} = Age_pV_{P\_h} + Age_{pas}V_{P\_pas} - Age_hET_h - Age_hQ_{h-s} - Age_hQ_{h-f} + Age_{pas}V_{pas\_in} - Age_hV_{pas\_in} \tag{10}$$

200   $$\frac{dAge_{pas}(V_{pas})}{dt} = Age_pV_{P\_pas} - Age_{pas}V_{P\_pas} + Age_hV_{pas\_in} - Age_{pas}V_{pas\_in} \tag{11}$$

where Age_{pas} is passive reservoir in hillslope.

Details of the modules within the model and related equations and parameters (highlighting those calibrated) are given in Appendix A. In the equations of each module shown in Table A1, fast and slow flow reservoir storages are drained by the calibrated linear rate parameters K_f and K_s (hour^{-1}), and the exchange flow between them is calculated using the parameter K_e

205 (hour^{-1}) and f (Table A2). Hillslope storage is drained by the exponent parameter w; precipitation recharging to the slow flow reservoir are calculated by the parameter a (and to the fast flow reservoir by 1-a); Hillslope lateral flow to the slow reservoir is calculated by the parameter b (to fast flow reservoir by 1-b); estimation of the effects of evaporative fractionation are considered by the parameter Is; Rainfall recharge to active and passive stores in the hillslope are calculated by the parameters KK and pp; Exchange flow between active and passive stores in hillslope is calculated by the parameter con; And the weighted

210 isotope composition of rainfall input is calculated by the parameter fei. The initial range for each of the parameters was set in Table 3.

Additionally, lateral surface flow can indirectly recharge into the fast reservoir through sinkholes in the depression in heavy rainfall event. According to research at Chenqi by Peng and Wang (2012), the mean surface runoff coefficient from the hillslopes are about 10% when the hourly rainfall amount exceeds 30mm. Hence, ten percent of rainfall infiltration of hillslope

215 will recharge to fast flow reservoir via sinkholes in this situation (rainfall amount >30 mm/hr).

3.2 Modelling procedure

Modelling started on 23 July 2016, but calibration was initiated using available discharge data only from 01 November 2016. The preceding three months were used as a spin-up period (the mean of precipitation isotope signatures over the sampling period was used for the spin-up period) to fill storages, initialise storage tracer concentrations, and minimize the effects of

220 initial conditions on water age calculations.

The modified Kling–Gupta efficiency (KGE) criterion (Kling et al., 2012) was used as the objective function for calibration. The KGE is a three dimensional representation (Euclidean distance) of the widely used Nash–Sutcliffe criterion, overcoming some weaknesses of the latter (Schaefli and Gupta, 2007) and balancing dynamics (correlation coefficient), bias (bias ratio) and variability (variability ratio). Using flow and isotopic composition as calibration targets, objective functions were

225 combined to formulate a single measure of goodness of fit: KGE= (KGE$_d$ + KGE$_i$) /2 (KGE$_d$ is for discharge, KGE$_i$ is for isotopic composition).

The time series of discharge and isotope data were different in length. The high-resolution samples for stable isotope composition were collected in 8 events from 12 June to 13 August, 2017, giving a total of 589 samples. Hence, the KGE$_d$ and KGE$_i$ were each calculated using the all available data for discharge and isotope ratios, respectively. A Monte Carlo analysis

230 was used to explore the parameter space during calibration (Table A2). In order to derive a more behavioural parameter set, two calibration iterations were carried out. First, 10^5 different parameter combinations within the initial ranges in Table 3 were tested. And then, the parameter ranges were reduced according to the best models (KGE >0.3) for the second calibration. This

resulted in a total of 10^5 tested different parameter combinations. Only the best (in terms of the efficiency statistics) parameter

populations (500 parameter sets) were retained and used for further analysis, which included calculation of simulation bounds

235   representing posterior parameter uncertainty. The retained 500 parameter sets were applied to simulate model output, and it

was assumed that the results provide a range of behavioral models indicative of the model uncertainty in the absence of a

formal uncertainty analysis similar to Birkel et al. (2015b). Additionally, available data such as the discharge and stable isotope

signatures of hillslope spring and isotopes in the depression wells were used as qualitative "soft" data to aid model evaluation.

A regional sensitivity analysis (Freer et al., 1996) was further used to identify the most important model parameters. The

240   parameter sets were split into 10 groups and ranked according to the selected objective function. For each group the likelihoods

were normalized by dividing by their total, and the cumulative frequency distribution was calculated and plotted. If the model

performance is sensitive to a particular parameter there will be a large difference between the cumulative frequency

distributions compared to a 1:1 line.

3.3 Line-conditioned excess

245   The lc-excess describes the deviation of a water sample from the Local Meteoric Water Line (LMWL) in dual-isotope space,

which indicates evaporation-driven kinetic fractionation of precipitation inputs (Sprenger et al., 2016; McCutcheon et al.,

2017). With a known LMWL of $\delta^2H = a * \delta^{18}O + b$, it was thus proposed by Landwehr and Coplen (2004) that: lc-excess =

$\delta^2H - a * \delta^{18}O - b$. As oxygen has a higher atomic weight, non-equilibrium fractionation during the liquid-to-vapour phase

change will preferentially evaporate (in terms of statistical expectation) $^1H^2H^{16}O$ molecules. The isotopic signature of a water

250   sample affected by evaporation thus shows negative lc-excess values, and plots under the LMWL in dual-isotope space

(Landwehr et al., 2014). The LMWL of $\delta^2H = 7.77 * \delta^{18}O + 4.88$ was defined based on a daily value set of isotope signature

at precipitation from August 2016 to September 2017 in Chenqi catchment. The calculated lc-excess values were shown in

Table 2.

4 Results

255   ### 4.1 Simulating flow and tracer dynamics

4.4.1 The simulated flow and tracer at catchment outlet

The initial parameter ranges are listed in Table 3, along with the mean of the 500 best simulations. For the analysis, the assumed

behavioural parameter sets retained from the best 500 runs were applied to simulate model outputs with an indication of

uncertainties. The model results show that the discharge and isotope dynamics were mostly captured by the simulation ranges

260   at the outlet, and though some peak discharges were underestimated (Figure 3). The objective function values of KEG at the

outlet were all greater than 0.65 for the best 500 parameter sets (Table 3). As is common in coupled flow-tracer models, the

performance in the simulation of isotope was more uncertain than for discharge; KEG_d ~0.8 compared with ~0.5 for KEG_i. In general isotope values in rainfall events depleted as the event progressed and this also depressed values in the underground stream, which the model generally reproduced (Figure 3).

265   The sensitive analysis results in Figure 4 show that fast flow reservoir constant (K_f), precipitation recharge coefficient for slow flow reservoir (a) and for fast flow reservoir ($1- a$), recharge coefficient of hillslope to slow flow reservoir (b) and to fast flow reservoir ($1- b$), coefficient for evaporation fractionation (Is) and weighting constant (fei) are generally more sensitive to the combined simulation of flow and isotopic composition.
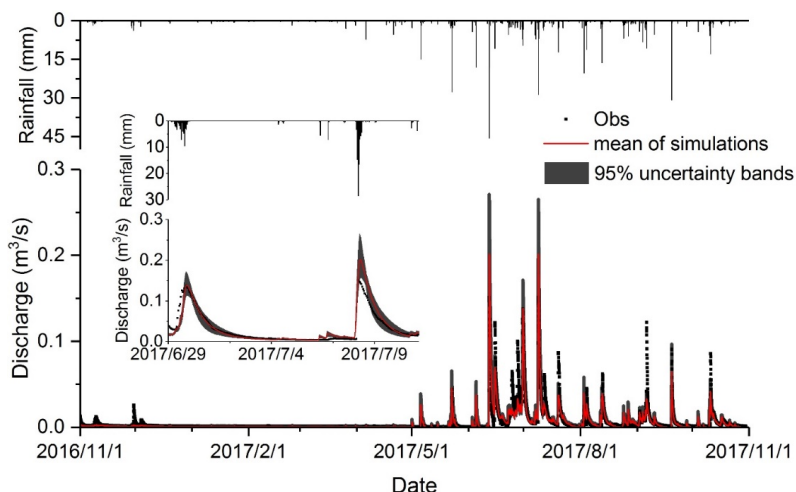
270   **(a) Observed and simulated stream discharge over the study period (inset shows higher resolution response over a 12 day period)**
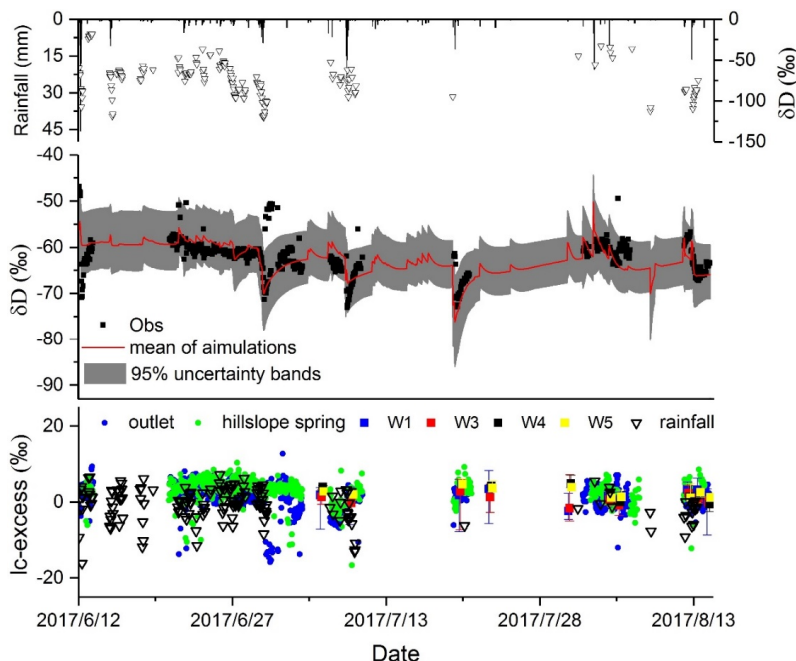
(b) Observed and simulated deuterium, and lc-excess values

Figure 3 Observed stream discharge and deuterium during the study period, and discharge and deuterium simulations for the best 500 parameter sets; and lc-excess values of rainfall, outlet, hillslope spring and depression wells

275 The results of isotope simulations showed that despite reproducing the general depletion, the model structure failed to capture some "rogue" high isotope values during event peaks where isotope values generally depleted (e.g. late June/early July 2017 in Figure 3). In order to explore this further, the line-conditioned excess (lc-excess) of samples was calculated from samples. The results of lc-excess values in Figure 3, with the mean of -0.59 and 1.13 at rainfall and outlet (Table 2), show a frequent evaporative fractionation effect in the underground stream over the sampling periods. Especially, there were a few samples

280 which showed markedly negative of lc-excess values around event peaks (e.g. 22/6, 1/7, and 5/8), indicating a strong fractionation effect. These outliers correspond to the "rogue" enriched isotope values that the model fails to capture.

The lc-excess of isotope time series of the hillslope spring and wells in the depression were estimated (Figure 3). The mean lc-excess values were also slightly negative (2.91, 1.72, 0.66, 2.37 and 2.39, respectively) for the hillslope spring, W1, W3, W4 and W5 for depression wells (Table 2), again indicating an evaporative fractionation effect on recharge water. However,

285 the underground stream flow (mainly reflecting the response of "fast flow" reservoirs) with the "rogue" high isotope values could not be attributed to the hillslope response or groundwater in the depression (the maximum of δD less than -50 in Table 2), because the lc-excess values of these sources were less negative than the simultaneous values of the underground stream (Figure 3) and the maximum of δD (-46.9) at outlet was larger than that at hillspring and depression wells (less than -50) in Table 2. The most likely explanation relates to flooded paddy fields which are extensively distributed in the depression during

290 the growing season. Consequently, large volumes of surface water are impounded in the paddy fields and exposed for evaporative fractionation. Therefore the markedly enriched isotope signals at the outlet around some event peaks would be consistent with fractionated water being displaced from the paddy fields and entering the fast flow system. This would explain the model's lack of skill in capturing such effects of evaporative fractionation.

Table 3 Mean parameter values and fitness derived from the best 500 parameter sets after calibration

For Flow	K_s (hour^{-1})	K_f (hour^{-1})	K_e (hour^{-1})	f	a	W	b
Initial range	40-150	1-40	800-2200	0.008-0.025	0.47-1	0-0.015	0.48-1
Mean	92	11	1549	0.015	0.68	0.005	0.54
Range	48-120	5-18	1000-2000	0.01-0.02	0.51-0.9	0.003-0.01	0.5-0.62

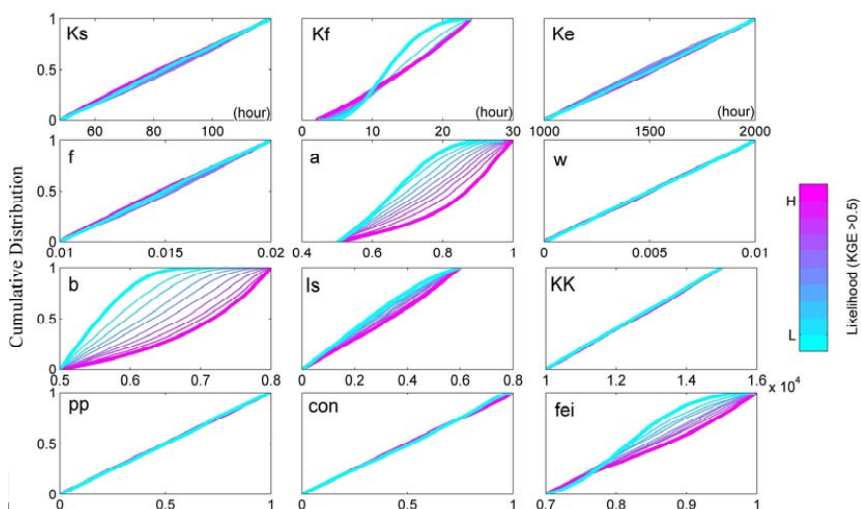| For Isotope	Is	KK (×10^4)	pp	con	fei	Index	Mean(range)
						KGE_d	0.85 (0.81-0.87)
Initial range	0-0.8	0.8-1.6	0-1	0-1	0.5-1	KGE_i	0.56 (0.52-0.59)
Mean	0.24	1.26	0.49	0.56	0.82	KGE	0.7 (0.72-0.66)
Range	0.002-0.6	1-1.5	0.02-0.95	0.04-0.97	0.71-0.93		

295

Figure 4 Sensitivity of 12 model parameters expressed as cumulative distributions in ten levels of likelihood values for the model simulations from the lowest likelihood value (blue) to the highest likelihood value (purple). Likelihood based on KEG and rejection of values <0.5.

4.4.2 The simulated flow and tracer for hillslope spring and depression wells

As a more qualitative indication of model performance, Figure 5 shows the normalized simulated discharge ($Q_n=Q_i/Q_{mean}$) of the hillslope unit had very similar seasonality and event-based dynamics to the normalized observed discharge at hillslope spring. The magnitude of the modelled discharge fluxes is, of course, different to those observed at the specific hillslope (e.g. HS at the east hillslope in Figure 1) because the simulation results represented the lumped outputs of the whole hillslope unit. However, as a "soft" validation of the model it adds confidence that the temporal dynamics of the hillslope response are appropriately captured.
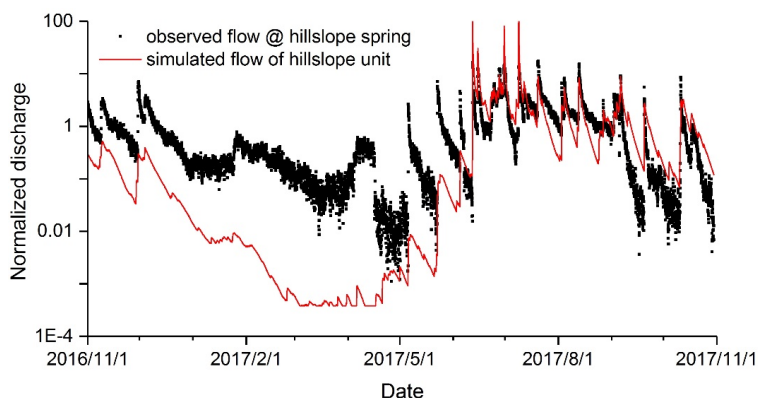

Figure 5 Observed discharge at hillslope spring (in Fig.1) against the simulated discharge of hillslope unit (mean of the simulations for the best 500 parameter sets). Note values are normalized.

310   A further qualitative test of the model was given by comparing the internal tracking of isotope dynamics in the conceptual

stores of the hillslope and slow flow reservoir with available from measured isotope values collected for the hillslope spring

and wells (Figure 6). The sampling frequency of the hillslope spring was same as at the outlet; however, there were only 10

sampling occasions from the well W1 over the dry and wet season, and the water samples were collected across a range of

depths of the well. Again, although these point measurements are not strictly comparable with the tracked isotope composition

315   of conceptual stores, they do give an indication of how plausible the internal states of the model are in terms of the mixing

volumes which damp the isotope inputs in precipitation. The results are encouraging, showing that the model can capture the

general directions of changes in the isotope dynamics of the hillslope spring (Figure 6a). The modelled isotope composition

of depression wells are relatively constant, however, measured values of W1 and W5 (blue and yellow points) are also

relatively constant and even samples collected at multiple depths generally have their variability bracketed within the modelled

320   uncertainty (Figure 6b). Recent geophysical surveys around the four wells (Chen et al, in review), show that there is relatively

low permeability rock around W1 and W5, and high permeability rock around W3 and W4. Hence, to some extent, the water

in W1 and W5 seems consistent with the slow reservoir water in depression. While the water in W3 and W4 (red and black

points in Figure 6b) are contributed by a mixing of flow from the slow and fast reservoir, especially during rainfall event (e.g.

9/7, and 20/7), leading to some samples being out of the modelled uncertainty.
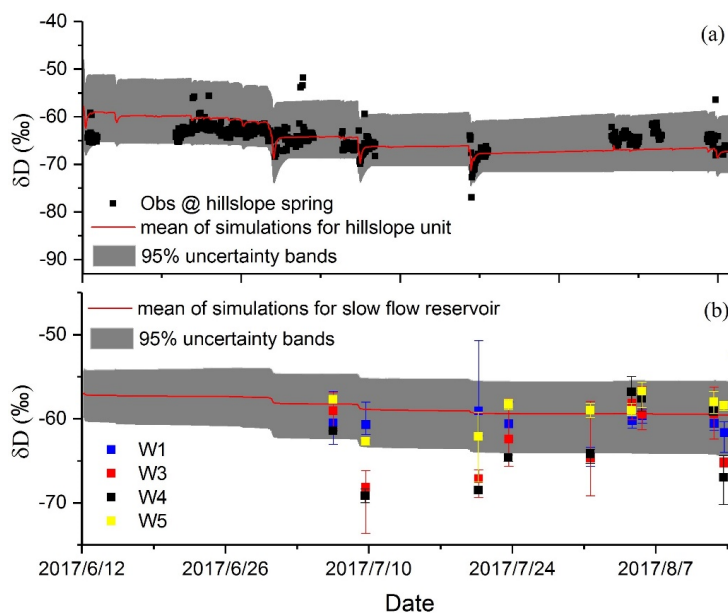
325

Figure 6 Modeled isotope signature at hillslope unit and slow reservoir vs observation at hillslope spring and depression wells (the red line represents mean of the simulations for the best 500 parameter sets).

4.2 Storage dynamics of different reservoirs and source contributions of underground stream flow

The storage dynamics of the catchment derived by the model in order to simulate the concurrent flow and tracer response can

330   be disaggregated according to conceptual stores (Figure 7). The model structure dictates that the main variability in the runoff

response to precipitation is driven by the storage dynamics, depending on hydrological connectivity between the hillslope (V_h),

slow (V_s) and fast (V_f) flow reservoirs (Figure 2). The modeled storage results show that slow flow reservoir was the largest

store in the catchment (~ >100mm with mean of 245 mm), consistent with the wide distribution of small fractures and matrix

pores in the karst critical zone (Zhang et al., 2011, 2017). The fast flow reservoir had the smallest storage (the mean value was

335   only 0.2mm) because the underground river/conduit volume represents only a very small proportion of the porosity of the

entire aquifer. Although the hillslopes cover a larger area than the depression, the thin soil, shallow epikarst and rapid drainage

resulted in a relatively small storage reservoir, with a calibrated mean value of 23mm. The discharge over the study period

showed clear seasonality, which reflects the uneven distribution of precipitation throughout the year (Figure 3). This

seasonality is mirrored somewhat differently in the storage dynamics of each reservoir (Figure 7). The storage change in fast

340   flow reservoir was very rapid, especially in the wet season; this reflects the rapid recharge and water release. The rapid response

of storage to rainfall was also evident in hillslope reservoir because of the low capacity and rapid response.
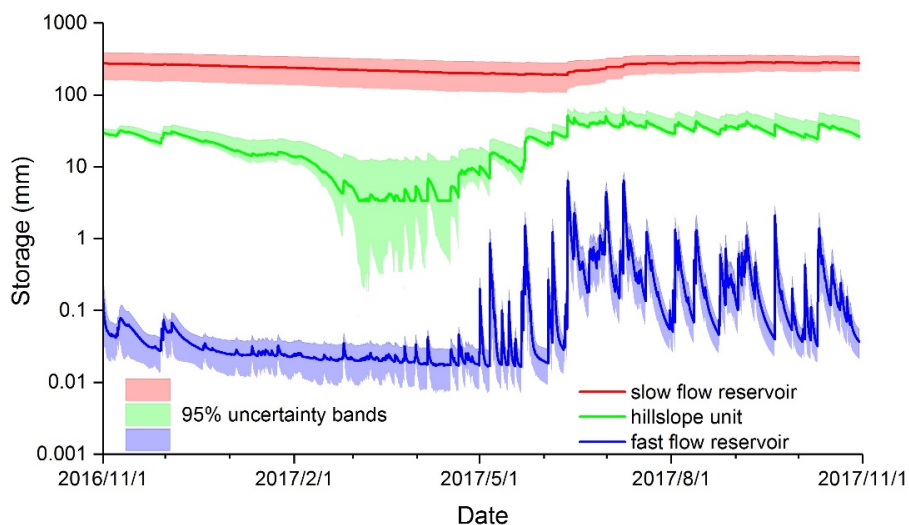

Figure 7 Model-derived storage dynamics in hillslope (V_h), slow (V_s) and fast (V_f) conceptual reservoirs for the best 500 parameter sets, and the lines represent the mean of simulations

345   The relative contributions of the different sources to stream flow changed with hydroclimatic conditions, and this could be

estimated using the calibrated model. Figure 8 shows that during the dry period (November 2016 to April 2017), underground

stream flow was mainly sustained from the small fractures (conceptualized as release from the slow flow reservoir). Overall,

this provided the largest proportion (78.4%) of dry season flows, followed by hillslope unit contribution (16.8%). During this

period, the rainfall infiltration contributed only limited water to the underground stream (4.8%) due to the low rainfall and

350   limited storage, resulting in weak hydrological connectivity between hillslope and depression. During the wet period, with the

resulting rapid increase in storage, the hillslope unit contributes much more water to the underground stream, accounting for

the largest proportion (57.5%) of overall flow, due to the strong hydrological connectivity between the hillslope and depression.

Meantime, the contribution of direct rainfall infiltration to the underground stream flow also increased (with an overall wet

season contribution of 35.6%). This likely reflects the increased influence of sinkholes and big fractures as the catchment

355   becomes wetter. In such conditions, during storm events, overland flow and epikarst water were collected by sinkholes and

large fractures and recharged to underground stream directly. The contribution rate of small fractures in the slow reservoir

decreased substantially (7%) although the overall magnitude of the water flux to the underground stream increased during wet

period.

The bi-directional exchange between the underground conduit and small fractures is a unique feature of the karst critical zone

360   (Zhang et al, 2017). During the dry period, as water table levels in the conduits drop more rapidly than in the smaller fractures,

water stored in the fractures drains into conduits and underground channels as baseflow. In the wet season, especially during

the periods of highest flow, infiltrated water quickly fills conduits where water table is higher than the adjacent fractures.

Water is temporarily stored in the conduits, and hence induces recharge in the small fractures. These bi-directional exchange

flows between the underground channels and small fractures were captured by this model (represented by fast and slow

365   reservoirs, respectively) and are shown in Figure 8, where the negative values represent the flux from conduits to small

fractures. This bi-directional flow was affected by the wetness conditions, being evident in the wet season and indicating both

the seasonal and short-term temporal change of hydrological connectivity between the fast and slow flow reservoirs.
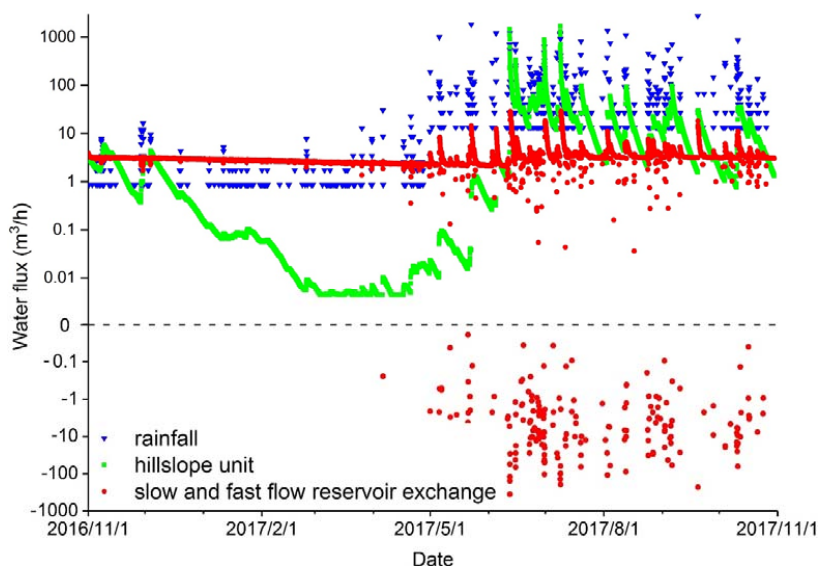
Figure 8 Source contributions to the underground stream flow (fast reservoir) at the catchment outlet (mean of the simulations for
370   **the best 500 parameter sets). The red dots above and under the dotted line represent transient reverse water fluxes from the slow**
reservoir to fast reservoir and fast reservoir to slow reservoir, respectively.

4.3 Simulated flux ages from different conceptual stores

The estimated ages of water fluxes from the different landscape units were tracked using the model. The simulated water ages were closely linked to the size of storage in each unit and the ages of the fluxes were hillslope reservoir< fast flow reservoir <

375   slow flow reservoir, with mean ages of 137, 326 and 493 days, respectively, and uncertainty increasing with age (Figure 9). The mean ages of water flux decreased between the dry and wet seasons: ranges from 159, 466 and 528 days for the dry season to 115, 187 and 458 days for the wet season, for the hillslope, fast flow and slow flow reservoirs respectively. The ages of fluxes from the fast flow reservoir in the underground stream generally reflected the integration of younger water fluxes from hillslope and older fluxes from the slow flow reservoir, as shown in the flux ages visualized in time series in Figure 9.

380   Consequently, the water age dynamics of the fast flow reservoir were relatively close to the slow flow reservoir in the dry season and close to hillslope reservoir in wet season as connectivity changed. This is consistent with the changing storage dynamics shown above. However, a distinct feature in Figure 9 is that the water ages in the fast flow reservoir were younger than which from hillslope reservoir during some events in the wet period. This again, most likely reflects the role of sinkholes in collecting water with a high proportion of new rainfall (young water) in intense wet season rain events and then recharging

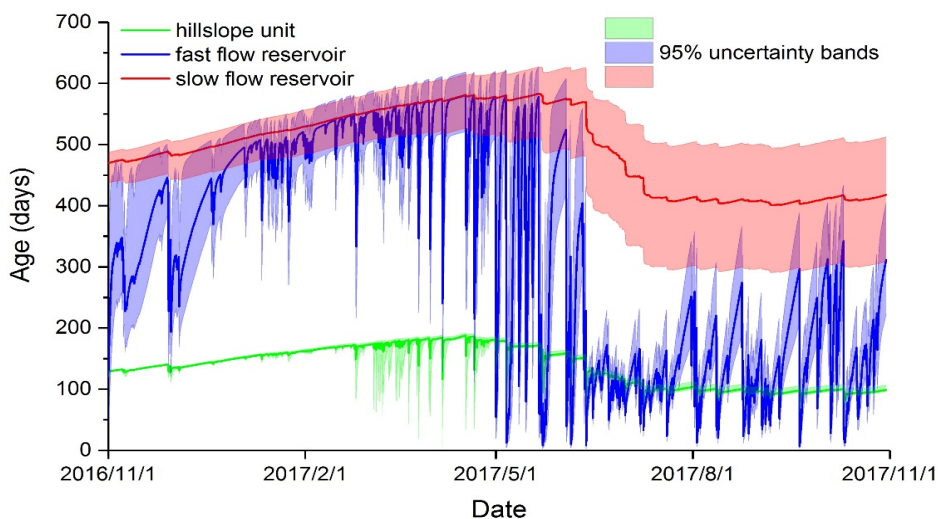385   underground stream rapidly due to the direct, transient connectivity.

Figure 9 Mean of water flux age of hillslope, fast and slow reservoir (for the 500 best parameter sets)

The probability density functions (PDFs) of the simulated flux ages from the three reservoirs are shown in Figure 10 (using the best 500 parameter sets). The ages of fluxes from the fast flow reservoir varied from a few days to over 600 days, and it is

390   clearly evident that the PDF was bimodal with peaks corresponding to water ages of ~100 and ~550 days. From the water age dynamics in Figure 9, it equally clear that the bimodal distribution of ages of underground stream flow reflected the seasonality of different water sources contributions in the wet and dry seasons. The underground stream flow was dominated by older water from the matrix and small fractures during the dry period and by younger hillslope fluxes during wet period, respectively.

The water age distributions for the hillslope also showed seasonal bimodality in flux ages, albeit less pronounced, though the

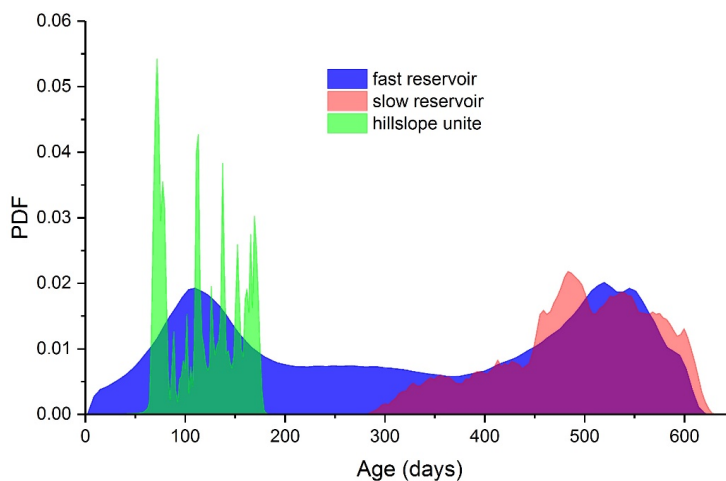395   model has also produced a less smooth distribution of more transient younger ages.

Figure 10 Probability density functions of the simulated water ages for the best 500 runs in fluxes for all three reservoirs

5 Discussion

400   **5.1 Using conceptual water-tracer model with low parameterization for karst catchments**

In karst areas, complex subsurface flow systems, with profound spatial heterogeneity in porosity and structure, and marked

temporal variations in hydrological connectivity, dictates that the karst critical zone is a particular challenge to hydrological

modelling. Process-based modelling is often difficult in such areas (e.g. Zhang et al, 2011; Doummar et al., 2012), because of

limited knowledge about the physical structure of subsurface drainage networks. Although conceptual modelling is more

405   simplistic, with relatively low parameterization, it can provide a framework for a reasonable, evidence-based first

approximation of the flow system. Hence, many conceptual models have been used in karst catchments in recent years

(Ladouche et al, 2014; Arfib and Charlier, 2016). However, high uncertainty always accompanies modelling in such complex

landscapes. The tracer-aided conceptual model used here provided an opportunity to improve the basis for model evaluation

and constrain parameter sets potentially reducing such uncertainty (Beven, 1993). Such an approach is helpful in karst regions,

410   because using isotope tracers as "fingerprints" means that hydrological processes can be tracked in a way that provides insights

into storage dynamics and can resolve "fast" and "slow" water fluxes and estimate their ages.

This is a significant advance on previous work, where we developed a dual-reservoir conceptual flow-tracer model for similar

conditions and calibrated the model on both flow and solute (Ca and Mg) concentrations in three nested karst catchments

(Zhang et al, 2017). However, the earlier model was unable to differentiate the flow, storage, and tracer dynamics of different

415 landscape units, or track water ages. The separation of the hillslope and depression in the current study improved model performance and was more informative in terms of the results showing clearly the flow and tracer dynamics within different landscape unit, as well as tracking spatially distributed storages and ages of water flux. Moreover, the model approach is potentially transferable to other cockpit karst catchments with similar landscape organization.

Although the model incorporates the effects of evaporative fractionation of water recharging the underground flow system by
420 a simple parameter, it can't capture some of the markedly enriched isotope signals at the outlet during the event peaks which are most likely explained by fractionated water being displaced from the paddy fields during event peaks. Hence, the skill in capturing the effects of evaporative fractionation need to be further investigated in the model; both in terms of process-based parameterisation of fractionation (e.g. Kuppel et al., 2018) and possibly differentiating paddy fields as a separate landscape unit. Though of course this would be a trade-off with increased parameterization.

425 **5.2 High temporal resolution isotope data for karst area**

There is a marked shift in the isotopic composition of storm event rainfall due thus weekly or even daily isotope data do not adequately capture the variability of rainfall isotope signatures at a resolution appropriate to the response times of karst systems (Coplen et al., 2008). The assessment of water ages in the critical zone is very dependent on the temporal resolution of tracer data in rainfall and stream flow for model conceptualization (Birkel et al., 2012; McDonne and Beven, 2014). The high-
430 frequency measurements of tracer behaviour enhanced our understanding of catchments' hydrological function and the associated time scales of hydrological response to rainfall inputs. Also, the high-resolution tracer data yielded novel insights into how the model integrates and aggregates the intrinsic complexity and heterogeneity of catchments, in order to reproduce behaviour adequately across a range of time scales (Kirchner et al., 2004). However, it should be noted that in much previous tracer-based modelling, the temporal resolution of hydrometric data (typically hourly) is at a much finer temporal resolution
435 than tracer data, sampled more often at daily or even weekly resolution (Stets et al., 2010; Birkel et al., 2010, 2011; McMillan et al., 2012; Soulsby et al., 2015; Ala-Aho et al., 2017a). Here, due to the marked heterogeneity of flow paths in the karst critical zone, and the very rapid (i.e. sub-daily) stream flow responses to high intensity precipitation, the modelling of flow and tracer dynamics, as well as flux age estimates, need to account for the rapid flow velocities within the karst aquifer. The response time of stream/conduit flow or groundwater level to rainfall is very short in karst catchments, e.g. typically a few
440 hours in small catchments like Chenqi (Zhang et al., 2013; Delbart et al., 2014; Labat and Mangin, 2015; Rathay et al., 2017). Coarser resolution data would result in increased uncertainty in the short-term components of travel times (Seeger and Weiler, 2014) and a likely bias towards longer transit times (Heidbuechel et al., 2012). Thus a significant advance in the study was that observation and model results captured the flashy (sub-daily) responses of flow and isotope signatures at hourly timescales.

5.3 Hydrological connectivity between different landscape units

445   Given the results on water storage dynamics and the relative contribution to the fast flow reservoir shown in Figures 7 and 8,

it can be deduced that the storage change within each conceptual stores is the main driver of hydrological connectivity between

them. During the dry period, there is weak hydrological connectivity between the hillslope and depression due to low storage.

In contrast, during the wet period, hydrological connectivity between the hillslope and depression strengthens as water storage

increases. In the early recession after heavy rain, large fractures in the hillslope fill, leading to large water fluxes into the

450   depression. Then, as storage declines, fluxes decrease and the hydrological connectivity weakens.

The hydrological connectivity and exchange between the slow and fast flow reservoirs is mainly controlled by the water level

of each medium, rather than the storage. The flow directionality will change with the hydraulic gradient between the two

reservoirs. Previously, few studies of hydrological connectivity have considered its directionality (e.g. Tetzlaff et al, 2007;

Lexartza-Artza and Wainwright, 2009; Bracken et al., 2013; Soulsby et al., 2015). The common indices of hydrological

455   connectivity used are: integral connectivity scale lengths (ICSL), semivariogram-derived metrics (Ali and Roy, 2010), critical

path conductivity (Knudby and Carrera, 2005), index of connectivity (Borselli et al., 2008), network index (Lane et al., 2009),

relative surface connection function (Antoine et al., 2009), and saturated area (Birkel et al., 2010). Which means hydrological

connectivity is usually treated as a scalar. However, the bidirectional water flux makes it fundamental to consider the

directionality of connectivity within the karst critical zone. Direct hydrological connectivity between the surface and

460   subsurface is also important in stream flow generation in karst catchments. Besides infiltration through fractures and the matrix,

concentrated infiltration from surface to underground flow systems via sinkholes is a unique aspect of transient connectivity

in karst catchments. This influence is clear from the contribution of rainfall to the underground stream in Figure 8. Although

this hydrological connection only occurs during heavy rain in the wet season, it is one of the most important hydrological

functions of the karst critical zone. In this regard flow paths in urban areas, with transient connectivity of storm drains, have

465   been compared to karst (Bonneau et al. 2017) ; and whilst this gives similar short response times and a dominance of young

water (Soulsby et al., 2014) urban systems are simpler and bi-directional connectivity is less significant.

5.4 Water ages of different conceptual stores

Through characterizing water ages of different landscape units, we can deepen our understanding of the non-linear water

storage dynamics and runoff generation processes (Soulsby et al, 2015). Water ages reflect the time variance and non-linearities

470   of how different runoff sources are connected and the dynamics of their relative contribution to runoff generation (Birkel et

al., 2012). Recent work has demonstrated the controlling effect of hydrogeological conditions on water ages in karst areas

(Mueller et al, 2013). The underground stream water ages at the catchment outlet can be viewed as the time-varying integration

of spatially distributed water fluxes from the hillslope unit and small fractures in the depression aquifer, which each have their

own age dynamics (Figure 9). There is a distinct pattern of bimodality in the age distribution of underground stream flow

475 (Figure 10), which reflects the seasonality of the different water sources. Younger waters mainly come from surface water

recharge through sinkholes after heavy rain and drainage from the hillslopes, whilst the low flow reservoir dominates low

flows. According to the water age dynamics of different conceptual stores, it can be deduced that storage-driven changes in

hydrological connectivity and associated mixing processes largely determine the nonstationary water age distribution of the

underground stream. In this sense, karst catchments seem to be subject to the "inverse storage effect", where periods of high

480 storage facilitate release of more younger water to drainage (Hartmann, 2014).

It should be noted that the ages derived from the modelling are based on stable isotope tracers, which whilst well-suited to

characterizing the influence of younger waters, are less well-suited to constraining the age of older waters (>5 years) that may

be present in deeper aquifers and fine pores that contribute to the slow flow reservoir (e.g. Jasceheko et al., 2017). Thus further

work is needed to assess the role of these older waters and quantify their influence on the ages of water in the older channel

485 (e.g. McDonnell and Beven, 2014). That said, the dominance of younger water in the outflow of responsive karst catchments

is consistent with recent theoretical (Berghuijs and Kirchner (2017), larger scale (Jasecheko et al., 2016) and more local studies

(Ala-aho et al., 2017b) which show that deeper, older groundwater makes limited contributions to stream flow.

5.5 The impacts of hydrological connectivity on the pollution vulnerability

Karst groundwater is known to be particularly sensitive to contamination, due to the aquifer structure and hydrologic behavior

490 (Hartmann et al 2013; Foster et al 2013). The characteristics of aquifer recharge, storage dynamics and young ages in dominant

water fluxes result in a high likelihood that pollutant transport will be very rapid with only limited attenuation (Zwahlen 2003).

Furthermore, during major recharge events (causing rapidly rising water tables) karst watersheds can exhibit radical changes

in their groundwater flow regime and connectivity. Land management on karst hillslopes has been associated with the

occurrence of diffuse pollution (Song et al., 2017). According to the results of our modelling, the hillslope is the dominant

495 contributor to the depression aquifer, when hydrological connectivity is high in the wet season. At the same time, any

contaminants will also be rapidly delivered into the depression. Hence, it is important to note that zones of depression aquifer

pollution vulnerability can be located at large distances from wells, encompassing surrounding hillslopes that can be directly

connected by lateral flow paths. The resulting water age distributions show that how dominant young waters are in hillslope

fluxes and the fast flow reservoir during the wet season. These can also be responsible for introducing pollution into the

500 underlying groundwater aquifer. The bi-directional exchange between fast and slow flow reservoirs potentially results in the

more matrix pollution in the slow reservoir, in the wet season. Consequently, the attenuation and recovery of matrix pollution

is very slow because of the low hydraulic conductivity. It is critical that the influence of sinkholes should be taken into account

when assessing pollution sensitivity in karst areas. It can be seen from the results of water ages in Figure 9 and 10 that sinkholes

facilitate the strong connectivity between the surface and ground water after heavy rain events. This potentially leads to more

505   pollutants entering the groundwater system and then being dispersed with the underground flows. These sensitivities need to

be recognized in restoration management of karst areas.

6 Conclusions

We extended a catchment-scale flow-tracer model for karst systems developed by Zhang, et al (2017) by conceptualizing two

main hydrological response units: hillslope and depression each containing fast and slow flow reservoirs. With this framework,

510   we could calibrate the model using high temporal resolution hydrometric and isotopic data to track hourly water and isotope

fluxes through a 1.25 km^2 karst catchment in southwest China. The model captured the flow and tracer dynamics within each

landscape unit quite well and we could estimate the storage, fluxes and age of water within each landscape unit. This inferred

that the fast flow reservoir had the smallest storage, the hillslope unit was intermediate, and the slow flow reservoir had the

largest. The estimated mean ages of the hillslope unit, fast and slow flow reservoirs were 137, 326 and 493 days, respectively.

515   Marked seasonal variability in hydroclimate and associated water storage dynamics were the main drivers of non-stationary

hydrological connectivity between the hillslope and depression. Meanwhile, the hydrological connectivity between the slow

and fast slow reservoirs had variable directionality, which was determined by the hydraulic head within each medium.

Sinkholes can make an important hydrological connectivity between surface water and underground stream flow after heavy

rain. New water recharges the underground stream via sinkholes, introducing younger water in the underground stream flow.

520   Whist the model here needs further development (e.g. the parameterization of isotopic fractionation in the paddy fields)

assessment and model validation requires longer and more detailed (e.g. better characterization of older waters) observation

data, it is an encouraging step forward in tracer-aided modelling of karst catchments.

Data availability. The isotope data as well as rainfall and flow measurements used for this paper are not publicly accessible

525   due to the constraints of governmental policy in China. The data were obtained through a purchasing agreement for this study.

GIS data in this study are available.

Author contributions. ZZ, XC, and CS conducted the modelling work and data interpretation, ZZ and QC conducted the field

and laboratory work, ZZ prepared the manuscript with contributions from co-authors.

530

Competing interests. The authors declare that they have no conflict of interest.

Hydrology and
Earth System
Sciences
Discussions
Open Access

References

540   Ala-Aho, P., Tetzlaff, D., McNamara, J. P., Laudon, H. and Soulsby, C.: Using isotopes to constrain water flux and age
estimates in snow-influenced catchments using the STARR (Spatially distributed Tracer-Aided Rainfall-Runoff) model,
Hydrol. Earth Syst. Sci., 21(10), 5089–5110, doi:10.5194/hess-21-5089-2017, 2017a.

Ala-aho, P., Soulsby, C., Wang, H. and Tetzlaff, D.: Integrated surface-subsurface model to investigate the role of groundwater
in headwater catchment runoff generation: A minimalist approach to parameterisation, J. Hydrol., 547, 664–677,
545   doi:10.1016/j.jhydrol.2017.02.023, 2017b.

Ali, G. A. and Roy, A. G.: Shopping for hydrologically representative connectivity metrics in a humid temperate forested
catchment, Water Resour. Res., 46(12), doi:10.1029/2010WR009442, 2010.

Antoine, M., Javaux, M. and Bielders, C.: What indicators can capture runoff-relevant connectivity properties of the micro-
topography at the plot scale?, Adv. Water Resour., 32(8), 1297–1310, doi:10.1016/j.advwatres.2009.05.006, 2009.

550   Arfib, B. and Charlier, J. B.: Insights into saline intrusion and freshwater resources in coastal karstic aquifers using a lumped
Rainfall–Discharge–Salinity model (the Port-Miou brackish spring, SE France), J. Hydrol., 540, 148–161,
doi:10.1016/j.jhydrol.2016.06.010, 2016.

Bakalowicz, M.: Karst groundwater: A challenge for new resources, Hydrogeol. J., 13(1), 148–160, doi:10.1007/s10040-004-
0402-9, 2005.

555   Berghuijs, W. R. and Kirchner, J. W.: The relationship between contrasting ages of groundwater and streamflow, Geophys.
Res. Lett., 44(17), 8925–8935, doi:10.1002/2017GL074962, 2017.

Beven, K.: Prophecy, reality and uncertainty in distributed hydrological modelling, Adv. Water Resour., 16(1), 41–51,
doi:10.1016/0309-1708(93)90028-E, 1993.

Beven, K.: A manifesto for the equifinality thesis, in Journal of Hydrology, vol. 320, pp. 18–36., 2006.

560   Birkel, C., Tetzlaff, D., Dunn, S. M. and Soulsby, C.: Towards a simple dynamic process conceptualization in rainfall-runoff
models using multi-criteria calibration and tracers in temperate, upland catchments, Hydrol. Process., 24(3), 260–275,
doi:10.1002/hyp.7478, 2010.

Birkel, C., Tetzlaff, D., Dunn, S. M. and Soulsby, C.: Using time domain and geographic source tracers to conceptualize
streamflow generation processes in lumped rainfall-runoff models, Water Resour. Res., 47(2), doi:10.1029/2010WR009547,
565   2011.

Birkel, C., Soulsby, C., Tetzlaff, D., Dunn, S. and Spezia, L.: High-frequency storm event isotope sampling reveals time-variant transit time distributions and influence of diurnal cycles, Hydrol. Process., 26(2), 308–316, doi:10.1002/hyp.8210, 2012.

Birkel, C. and Soulsby, C.: Advancing tracer-aided rainfall-runoff modelling: A review of progress, problems and unrealised potential, Hydrol. Process., 29(25), 5227–5240, doi:10.1002/hyp.10594, 2015a.

Birkel, C., Soulsby, C. and Tetzlaff, D.: Conceptual modelling to assess how the interplay of hydrological connectivity, catchment storage and tracer dynamics controls nonstationary water age estimates, Hydrol. Process., 29(13), 2956–2969, doi:10.1002/hyp.10414, 2015b.

Bonneau, J., Fletcher, T. D., Costelloe, J. F. and Burns, M. J.: Stormwater infiltration and the "urban karst" – A review, J. Hydrol., 552, 141–150, doi:10.1016/j.jhydrol.2017.06.043, 2017.

Borselli, L., Cassi, P. and Torri, D.: Prolegomena to sediment and flow connectivity in the landscape: A GIS and field numerical assessment, Catena, 75(3), 268–277, doi:10.1016/j.catena.2008.07.006, 2008.

Bracken, L. J., Wainwright, J., Ali, G. A., Tetzlaff, D., Smith, M. W., Reaney, S. M. and Roy, A. G.: Concepts of hydrological connectivity: Research approaches, Pathways and future agendas, Earth-Science Rev., 119, 17–34, doi:10.1016/j.earscirev.2013.02.001, 2013.

Charlier, J. B., Bertrand, C. and Mudry, J.: Conceptual hydrogeological model of flow and transport of dissolved organic carbon in a small Jura karst system, J. Hydrol., 460–461, 52–64, doi:10.1016/j.jhydrol.2012.06.043, 2012.

Chen, X., Zhang, Z.C., Soulsby, C., Cheng, Q.B., Binley, A., Jiang, R. and Tao, M.: Characterizing the heterogeneity of karst critical zone and its hydrological function: an integrated approach, Hydrol. Process.,In review, 2018.

Coplen, T. B., Neiman, P. J., White, A. B., Landwehr, J. M., Ralph, F. M. and Dettinger, M. D.: Extreme changes in stable hydrogen isotopes and precipitation characteristics in a landfalling Pacific storm, Geophys. Res. Lett., 35(21), doi:10.1029/2008GL035481, 2008.

Delbart, C., Valdes, D., Barbecot, F., Tognelli, A., Richon, P. and Couchoux, L.: Temporal variability of karst aquifer response time established by the sliding-windows cross-correlation method, J. Hydrol., 511, 580–588, doi:10.1016/j.jhydrol.2014.02.008, 2014.

Dewaide, L., Bonniver, I., Rochez, G. and Hallet, V.: Solute transport in heterogeneous karst systems: Dimensioning and estimation of the transport parameters via multi-sampling tracer-tests modelling using the OTIS (One-dimensional Transport with Inflow and Storage) program, J. Hydrol., 534, 567–578, doi:10.1016/j.jhydrol.2016.01.049, 2016.

Doummar, J., Sauter, M. and Geyer, T.: Simulation of flow processes in a large scale karst system with an integrated catchment model (Mike She) - Identification of relevant parameters influencing spring discharge, J. Hydrol., 426–427, 112–123, doi:10.1016/j.jhydrol.2012.01.021, 2012.

Field, M. S. and Pinsky, P. F.: A two-region nonequilibrium model for solute transport in solution conduits in karstic aquifers, J. Contam. Hydrol., 44(3–4), 329–351, doi:10.1016/S0169-7722(00)00099-1, 2000.

Fleury, P., Plagnes, V. and Bakalowicz, M.: Modelling of the functioning of karst aquifers with a reservoir model: Application
600   to Fontaine de Vaucluse (South of France), J. Hydrol., 345(1–2), 38–49, doi:10.1016/j.jhydrol.2007.07.014, 2007.

Ford, D. and Williams, P.: Karst Hydrogeology and Geomorphology., 2013.

Foster, S., Hirata, R. and Andreo, B.: The aquifer pollution vulnerability concept: aid or impediment in promoting groundwater protection?, Hydrogeol. J., 21(7), 1389–1392, doi:10.1007/s10040-013-1019-7, 2013.

Freer, J., Beven, K. and Ambroise, B.: Bayesian estimation of uncertainty in runoff prediction and the value of data: An
605   application of the GLUE approach, Water Resour. Res., 32(7), 2161–2173, doi:10.1029/96WR03723, 1996.

Fu, Z., Chen, H., Xu, Q., Jia, J., Wang, S. and Wang, K.: Role of epikarst in near-surface hydrological processes in a soil mantled subtropical dolomite karst slope: Implications of field rainfall simulation experiments, Hydrol. Process., 30(5), 795–811, doi:10.1002/hyp.10650, 2016.

Golden, H. E., Lane, C. R., Amatya, D. M., Bandilla, K. W., Raanan Kiperwas, H., Knightes, C. D. and Ssegane, H.:
610   Hydrologic connectivity between geographically isolated wetlands and surface water systems: A review of select modeling methods, Environ. Model. Softw., 53, 190–206, doi:10.1016/j.envsoft.2013.12.004, 2014.

Goldscheider, N., Meiman, J., Pronk, M. and Smart, C.: Tracer tests in karst hydrogeology and speleology, Int. J. Speleol., 37(1), 27–40, doi:10.5038/1827-806X.37.1.3, 2008.

Hartmann, A., Wagener, T., Rimmer, A., Lange, J., Brielmann, H. and Weiler, M.: Testing the realism of model structures to
615   identify karst system processes using water quality and quantity signatures, Water Resour. Res., 49(6), 3345–3358, doi:10.1002/wrcr.20229, 2013.

Hartmann, A., Goldscheider, N., Wagener, T., Lange, J. and Weiler, M.: Karst water resources in a changing world: Review of hydrological modeling approaches, Rev. Geophys., 52(3), 218–242, doi:10.1002/2013RG000443, 2014.

Hrachowitz, M., Savenije, H., Bogaard, T. A., Tetzlaff, D. and Soulsby, C.: What can flux tracking teach us about water age
620   distribution patterns and their temporal dynamics?, Hydrol. Earth Syst. Sci., 17(2), 533–564, doi:10.5194/hess-17-533-2013, 2013.

Jasechko, S., Kirchner, J. W., Welker, J. M. and McDonnell, J. J.: Substantial proportion of global streamflow less than three months old, Nat. Geosci., 9(2), 126–129, doi:10.1038/ngeo2636, 2016.

Jasechko, S., Perrone, D., Befus, K. M., Bayani Cardenas, M., Ferguson, G., Gleeson, T., Luijendijk, E., McDonnell, J. J.,
625   Taylor, R. G., Wada, Y. and Kirchner, J. W.: Global aquifers dominated by fossil groundwaters but wells vulnerable to modern contamination, Nat. Geosci., 10(6), 425–429, doi:10.1038/ngeo2943, 2017.

Jencso, K. G., McGlynn, B. L., Gooseff, M. N., Bencala, K. E. and Wondzell, S. M.: Hillslope hydrologic connectivity controls riparian groundwater turnover: Implications of catchment structure for riparian buffering and stream water sources, Water Resour. Res., 46(10), doi:10.1029/2009WR008818, 2010.

630   Jukic, D. and Denić-Jukić, V.: Groundwater balance estimation in karst by using a conceptual rainfall – runoff model, J. Hydrol., 373(3–4), 302–315, doi:10.1016/j.jhydrol.2009.04.035, 2009.

Kirchner, J. W.: A double paradox in catchment hydrology and geochemistry, Hydrol. Process., 17(4), 871–874, doi:10.1002/hyp.5108, 2003.

Kirchner, J. W., Feng, X., Neal, C. and Robson, A. J.: The fine structure of water-quality dynamics: The (high-frequency)
635   wave of the future, Hydrol. Process., 18(7), 1353–1359, doi:10.1002/hyp.5537, 2004.

Kling, H., Fuchs, M. and Paulin, M.: Runoff conditions in the upper Danube basin under an ensemble of climate change scenarios, J. Hydrol., 424–425, 264–277, doi:10.1016/j.jhydrol.2012.01.011, 2012.

Knudby, C. and Carrera, J.: On the relationship between indicators of geostatistical, flow and transport connectivity, Adv. Water Resour., 28(4), 405–421, doi:10.1016/j.advwatres.2004.09.001, 2005.

640   Kogovsek, J. and Petric, M.: Solute transport processes in a karst vadose zone characterized by long-term tracer tests (the cave system of Postojnska Jama, Slovenia), J. Hydrol., 519(PA), 1205–1213, doi:10.1016/j.jhydrol.2014.08.047, 2014.

Kübeck, C., Maloszewski, P. J. and Benischke, R.: Determination of the conduit structure in a karst aquifer based on tracer data-Lurbach system, Austria, Hydrol. Process., 27(2), 225–235, doi:10.1002/hyp.9221, 2013.

Kuppel, S., Tetzlaff, D., Maneta, M. and Soulsby, C.: EcH2O-iso: Water isotopes and age tracking in a process-based,
645   distributed ecohydrological model, Geoscientific Model Development, In review, 2018.

Labat, D. and Mangin, A.: Transfer function approach for artificial tracer test interpretation in karstic systems, J. Hydrol., 529, 866–871, doi:10.1016/j.jhydrol.2015.09.011, 2015.

Ladouche, B., Marechal, J. C. and Dorfliger, N.: Semi-distributed lumped model of a karst system under active management, J. Hydrol., 509, 215–230, doi:10.1016/j.jhydrol.2013.11.017, 2014.

650   Landwehr, J. and Coplen, T.: Line-conditioned excess: a new method for characterizing stable hydrogen and oxygen isotope ratios in hydrologic systems, in Aquatic Forum 2004: International conference on isotopes in environmental studies, p. 132–134. [online] Available from: http://dx.doi.org/10.8/S, 2004.

Landwehr, J. M., Coplen, T. B. and Stewart, D. W.: Spatial, seasonal, and source variability in the stable oxygen and hydrogen isotopic composition of tap waters throughout the USA, Hydrol. Process., 28(21), 5382–5422, doi:10.1002/hyp.10004, 2014.

655   Lane, S. N., Reaney, S. M. and Heathwaite, A. L.: Representation of landscape hydrological connectivity using a topographically driven surface flow index, Water Resour. Res., 45(8), doi:10.1029/2008WR007336, 2009.

Hydrology and
Earth System
Sciences
Open Access
Discussions
EGU

Legout, A., Legout, C., Nys, C. and Dambrine, E.: Preferential flow and slow convective chloride transport through the soil of a forested landscape (Fougères, France), Geoderma, 151(3–4), 179–190, doi:10.1016/j.geoderma.2009.04.002, 2009.

Lexartza-Artza, I. and Wainwright, J.: Hydrological connectivity: Linking concepts with practical implications, Catena, 79(2),
660   146–152, doi:10.1016/j.catena.2009.07.001, 2009.

McCutcheon, R. J., McNamara, J. P., Kohn, M. J. and Evans, S. L.: An evaluation of the ecohydrological separation hypothesis in a semiarid catchment, Hydrol. Process., 31(4), 783–799, doi:10.1002/hyp.11052, 2017.

McDonnell, J. J. and Beven, K.: Debates - The future of hydrological sciences: A (common) path forward? A call to action aimed at understanding velocities, celerities and residence time distributions of the headwater hydrograph, Water Resour. Res.,
665   50(6), 5342–5350, doi:10.1002/2013WR015141, 2014.

McGuire, K. J. and McDonnell, J. J.: Hydrological connectivity of hillslopes and streams: Characteristic time scales and nonlinearities, Water Resour. Res., 46(10), doi:10.1029/2010WR009341, 2010.

McMillan, H., Tetzlaff, D., Clark, M. and Soulsby, C.: Do time-variable tracers aid the evaluation of hydrological model structure? A multimodel approach, Water Resour. Res., 48(5), doi:10.1029/2011WR011688, 2012.

670   Morales, T., Uriarte, J. A., Olazar, M., Antigüedad, I. and Angulo, B.: Solute transport modelling in karst conduits with slow zones during different hydrologic conditions, J. Hydrol., 390(3–4), 182–189, doi:10.1016/j.jhydrol.2010.06.041, 2010.

Mudarra, M., Andreo, B., Marín, A. I., Vadillo, I. and Barberá, J. A.: Combined use of natural and artificial tracers to determine the hydrogeological functioning of a karst aquifer: the Villanueva del Rosario system (Andalusia, southern Spain), Hydrogeol. J., 22(5), 1027–1039, doi:10.1007/s10040-014-1117-1, 2014.

675   Mueller, M. H., Weingartner, R. and Alewell, C.: Importance of vegetation, topography and flow paths for water transit times of base flow in alpine headwater catchments, Hydrol. Earth Syst. Sci., 17(4), 1661–1679, doi:10.5194/hess-17-1661-2013, 2013.

Peng, T. and Wang, S.: Effects of land use, land cover and rainfall regimes on the surface runoff and soil loss on karst slopes in southwest China, CATENA, 90, 53–62, doi:10.1016/j.catena.2011.11.001, 2012.

680   Perrin, C., Michel, C. and Andréassian, V.: Does a large number of parameters enhance model performance? Comparative assessment of common catchment model structures on 429 catchments, J. Hydrol., 242(3–4), 275–301, doi:10.1016/S0022-1694(00)00393-0, 2001.

Rathay, S. Y., Allen, D. M. and Kirste, D.: Response of a fractured bedrock aquifer to recharge from heavy rainfall events, J. Hydrol., doi:10.1016/j.jhydrol.2017.07.042, 2017.

685   Rimmer, A. and Salingar, Y.: Modelling precipitation-streamflow processes in karst basin: The case of the Jordan River sources, Israel, J. Hydrol., 331(3–4), 524–542, doi:10.1016/j.jhydrol.2006.06.003, 2006.

Rimmer, A. and Hartmann, A.: Simplified Conceptual Structures and Analytical Solutions for Groundwater Discharge Using Reservoir Equations, Water Resour. Manag. Model., 2, 217–238, doi:10.5772/34803, 2012.

Schaefli, B. and Gupta, H. V.: Do Nash values have value?, Hydrol. Process., 21(15), 2075–2080, doi:10.1002/hyp.6825, 2007.

690   Seeger, S. and Weiler, M.: Lumped convolution integral models revisited: on the meaningfulness of inter catchment comparisons, Hydrol. Earth Syst. Sci. Discuss., 11(6), 6753–6803, doi:10.5194/hessd-11-6753-2014, 2014.

Song, X., Gao, Y., Green, S. M., Dungait, J. A. J., Peng, T., Quine, T. A., Xiong, B., Wen, X. and He, N.: Nitrogen loss from karst area in China in recent 50 years: An in-situ simulated rainfall experiment's assessment, Ecol. Evol., 7(23), 10131–10142, doi:10.1002/ece3.3502, 2017.

695   Soulsby, C., Birkel, C. and Tetzlaff, D.: Assessing urbanization impacts on catchment transit times, Geophys. Res. Lett., 41(2), 442–448, doi:10.1002/2013GL058716, 2014.

Soulsby, C., Birkel, C., Geris, J., Dick, J., Tunaley, C. and Tetzlaff, D.: Stream water age distributions controlled by storage dynamics and nonlinear hydrologic connectivity: Modeling with high-resolution isotope data, Water Resour. Res., 51(9), 7759–7776, doi:10.1002/2015WR017888, 2015.

700   Sprenger, M., Leistert, H., Gimbel, K. and Weiler, M.: Illuminating hydrological processes at the soil-vegetation-atmosphere interface with water stable isotopes, Rev. Geophys., 54(3), 674–704, doi:10.1002/2015RG000515, 2016.

Stets, E. G., Winter, T. C., Rosenberry, D. O. and Striegl, R. G.: Quantification of surface water and groundwater flows to open - and closed-basin lakes in a headwaters watershed using a descriptive oxygen stable isotope model, Water Resour. Res., 46(3), doi:10.1029/2009WR007793, 2010.

705   Tetzlaff, D., Soulsby, C., Bacon, P. J., Youngson, A. F., Gibbins, C. and Malcolm, I. A.: Connectivity between landscapes and riverscapes—a unifying theme in integrating hydrology and ecology in catchment science?, Hydrol. Process., 21(10), 1385–1389, doi:10.1002/hyp.6701, 2007.

Tetzlaff, D., Birkel, C., Dick, J., Geris, J. and Soulsby, C.: Storage dynamics in hydropedological units control hillslope connectivity, runoff generation, and the evolution of catchment transit time distributions, Water Resour. Res., 50(2), 969–985,

710   doi:10.1002/2013WR014147, 2014.

Tritz, S., Guinot, V. and Jourde, H.: Modelling the behaviour of a karst system catchment using non-linear hysteretic conceptual model, J. Hydrol., 397(3–4), 250–262, doi:10.1016/j.jhydrol.2010.12.001, 2011.

van Schaik, N. L. M. B., Schnabel, S. and Jetten, V. G.: The influence of preferential flow on hillslope hydrology in a semi-arid watershed (in the Spanish Dehesas), Hydrol. Process., 22(18), 3844–3855, doi:10.1002/hyp.6998, 2008.

715   White, W. B.: A brief history of karst hydrogeology: contributions of the NSS, J. Cave Karst Stud., 69(1), 13–26, doi:PNR61, 2007.

Hydrology and
Earth System
Sciences

Open Access

EGU

Discussions

Worthington, S. R. H.: Diagnostic hydrogeologic characteristics of a karst aquifer (Kentucky, USA), Hydrogeol. J., 17(7),

1665–1678, doi:10.1007/s10040-009-0489-0, 2009.

Zhang, Z., Chen, X., Ghadouani, A. and Shi, P.: Modelling hydrological processes influenced by soil, rock and vegetation in

720   a small karst basin of southwest China, Hydrol. Process., 25(15), 2456–2470, doi:10.1002/hyp.8022, 2011.

Zhang, Z., Chen, X., Chen, X. and Shi, P.: Quantifying time lag of epikarst-spring hydrograph response to rainfall using

correlation and spectral analyses, Hydrogeol. J., 21(7), 1619–1631, doi:10.1007/s10040-013-1041-9, 2013.

Zhang, Z., Chen, X. and Soulsby C.: Catchment-scale conceptual modelling of water and solute transport in the dual flow

system of the karst critical zone, Hydrol. Process., 31 (19): 3421–3436, doi: 10.1002/hyp.11268, 2017.

725   Zwahlen, F.: COST Action 620 Vulnerability and Risk Mapping for the Protection of Carbonate (Karst) Aquifers Final Report.,

2003.

Appendix A

Table A1 Algorithms in this model involving hydrological and isotopic modules. Note that the calibrated parameters are shown in red at the first appearance.

$P_h = P * Area_h/Area$ $P_s = (P-P_h) *a$ $P_f = (P-P_h) * (1-a)$	$Area_h$ and Area represent the hillslope and catchment area, respectively. Identify the areas using GIS.
$ET = \eta*ETP$ $ET_h = ET* Area_h/Area$ $ET_f = ET* (1- ET_h)*a$ $ET_s = ET* (1- ET_h) * (1-a)$	Potential evapotranspiration, ETP was calculated by Penman formula. Conversion factor η was from other study in this region.
$Q_{h,t} = w*exp(V_{h,t}/5000)$ $Q_{h-f, t} = b*Q_{h, t}$ $Q_{h-s, t} = (1-b) *Q_{h, t}$ $V_{h,t} = V_{h,t-1} + P_{h,t} - ET_{h,t} - Q_{h-f, t} - Q_{h-s, t}$	Porosity decreases with increasing depth Subscript t represents time
$\delta D_{h,t} = (\delta D_{h,t-1} * V_{h,t-1} * (1-con) + \delta D_{pas,t-1}* V_{h,t-1} * con + \delta D_{p,t} * P_{h,t} * Par_t + \delta D_{pas,t}*P_{h,t} * (1-Par_t) - \delta D_{h,t-1} * ET_{h,t} - \delta D_{h,t-1}* (Q_{h-f, t} + Q_{h-s, t}))/ V_{h,t}$	Useing the dynamic partial mixing method (Hrachowitz et al 2013) to calculate the isotope at hillslope
$\delta D_{pas,t} = (\delta D_{pas,t-1} * V_{pas,t-1} + \delta D_{p,t} * P_{h,t} * (1-Par_t) + \delta D_{h,t-1}* V_{h,t-1}* (1-con) - \delta D_{pas,t}* V_{h,t-1} * (1-con) – (1+ls)*\delta D_{pas,t-1} * ET_{h,t}) / (V_{pas,t} + P_{h,t} * (1-Par_t))$ $Par_t = pp* exp(V_{h,t}/kk)$	
$Age_{h,t} = (Age_{h,t-1}+1)* V_{h,t-1} * (1-con) + (Age_{pas,t-1}+1)* V_{h,t-1}* con + Age_{p,t} * P_{h,t} * Par_t + Age_{pas,t}*P_{h,t} * (1-Par_t) – (Age_{h,t-1}+1)*ET_{h,t} - (Age_{h,t-1}+1)*(Q_{h-f, t} + Q_{h-s, t}))/ V_{h,t}$	The Age of rainfall, $Age_{p,t}$, equal to 0.
$Age_{pas,t} = (Age_{pas,t-1}+1) * V_{pas,t} + Age_{p,t} * P_{h,t} * (1-Par_t) + (Age_{h,t-1}+1)* V_{h,t-1} * (1-con) - (Age_{pas,t-1}+1)* V_{h,t-1}$	

Hydrology and
Earth System
Sciences
Open Access
Discussions
EGU

$* (1\text{-con}) - (1+I_s) * (Age_{pas,t-1}+1) * ET_{h,t} / (V_{pas,t} + P_{h,t}$ $* (1\text{-}Par_t))$	
$Q_{s,t}=\Phi_{s,1}(I_{s,t}+Q_{h\text{-}s,t})+\Phi_{s,2}\Phi_{s,1}(I_{s,t-1}+Q_{h\text{-}s,t-1})+\Phi^2_{s,2}\Phi_{s,1}(I_{s,t-2}$ $+Q_{h\text{-}s,t-2}) + \Phi^2_{s,2}Q_{s,t-2} + \Phi_{s,3}Q_{f,t} + \Phi_{s,2}\Phi_{s,3}Q_{f,t-1} + \Phi^2_{s,2}\Phi_{s,3}$ $Q_{f,t-2} -\Phi_{s,1}ET_{s,t}$	
$Q_{f,t} =\Phi_{f,1}(I_{f,t}+Q_{h\text{-}f,t}) + \Phi_{f,2}Q_{f,t-1} +\Phi_{f,3}(\Phi_{s,1}I_{s,t}+\Phi_{s,2}\Phi_{s,1}I_{s,t-1}$ $+\Phi^2_{s,2}\Phi_{s,1}I_{s,t-2} +\Phi^2_{s,2}Q_{s,t-2} +\Phi_{s,3}Q_{f,t} +\Phi_{s,2}\Phi_{s,3}Q_{f,t-1} +$ $\Phi^2_{s,2}\Phi_{s,3}Q_{f,t-2})- \Phi_{f,1} ET_{f,t}$	
$\delta D_{p\text{-}d} = fei * \delta D_p$ $\delta D_{s,t}=\{\Phi_{s,1}(\delta D_{p\text{-}d,t}I_{s,t}+\delta D_{h,t}Q_{h\text{-}s,t})+\Phi_{s,2}\Phi_{s,1}(\delta D_{p\text{-}d,t-1}I_{s,t-1}+\delta D_{h,t-1}Q_{h\text{-}s,t-1})+\Phi^2_{s,2}\Phi_{s,1}(\delta D_{p\text{-}d,t-2}I_{s,t-2} +\delta D_{h,t-2}Q_{h\text{-}s,t-2}) +$ $\Phi^2_{s,2}\delta D_{s,t-2}Q_{s,t-2} + \Phi_{s,3}\delta D_{f,t}Q_{f,t} + \Phi_{s,2}\Phi_{s,3}\delta D_{f,t-1}Q_{f,t-1} +$ $\Phi^2_{s,2}\Phi_{s,3} \delta D_{f,t-2}Q_{f,t-2} -\Phi_{s,1}\delta D_{s,t-1}ET_{s,t}\}/Q_{s,t}$ $\delta D_{f,t}=\{\Phi_{f,1}(\delta D_{p\text{-}d,t}I_{f,t}+\delta D_{h,t}Q_{h\text{-}f,t})+\Phi_{f,2}\delta D_{f,t-1}Q_{f,t-1}+$ $\Phi_{f,3}(\Phi_{s,1}\delta D_{p\text{-}d,t}I_{s,t}+\Phi_{s,2}\Phi_{s,1}\delta D_{p\text{-}d,t-1}I_{s,t-1} +\Phi^2_{s,2}\Phi_{s,1}\delta D_{p\text{-}d,t-2}I_{s,t-2} +\Phi_{s,3}\delta D_{f,t}Q_{f,t} +\Phi_{s,2}\Phi_{s,3}\delta D_{f,t-1}Q_{f,t-1} + \Phi^2_{s,2}\Phi_{s,3}\delta D_{f,t-2}Q_{f,t-2}) - \Phi_{f,1} \delta D_{f,t-1}ET_{f,t}\}/(Q_{f,t} -\Phi_{f,3}\Phi_{s,3} Q_{s,t-2})$	Full derivation process in Zhang et al., 2017
$\Phi_{s,1} = 1/(K_s+fK_s/K_e)$ $\Phi_{f,1} = 1/(K_f+K_f/K_e+1)$ $\Phi_{s,2} = K_s/(K_s+ fK_s/K_e)$ $\Phi_{f,2} = K_f/(K_f+K_f/K_e+1)$ $\Phi_{s,3} = K_f/(K_sK_e+fK_s)$ $\Phi_{f,3} = fK_s/\{K_e(K_f+K_f/K_e+1)\}$	
$Age_{s,t}=\{\Phi_{s,1}(Age_{p,t}I_{s,t}+Age_{h,t}Q_{h\text{-}s,t})+\Phi_{s,2}\Phi_{s,1}((Age_{h,t-1}+1)I_{s,t-1}+(Age_{h,t-1}+1)Q_{h\text{-}s,t-1})+\Phi^2_{s,2}\Phi_{s,1}((Age_{p,t-2}+2)I_{s,t-2}$ $+(Age_{h,t-2}+2)Q_{h\text{-}s,t-2})+\Phi^2_{s,2}(Age_{s,t-2}+2)Q_{s,t-2}+$ $\Phi_{s,3}Age_{f,t}Q_{f,t} + \Phi_{s,2}\Phi_{s,3}(Age_{f,t-1}+1)Q_{f,t-1} + \Phi^2_{s,2}\Phi_{s,3}$ $(Age_{f,t-2}+2)Q_{f,t-2} -\Phi_{s,1}(Age_{s,t-1}+1)ET_{s,t}\}/Q_{s,t}$	
$Age_{f,t}=\{\Phi_{f,1}(Age_{p,t}I_{f,t}+Age_{h,t}Q_{h\text{-}f,t})+\Phi_{f,2}(Age_{f,t-1}+1)Q_{f,t-1}$ $+\Phi_{f,3}(\Phi_{s,1}Age_{p,t}I_{s,t}+\Phi_{s,2}\Phi_{s,1}(Age_{p,t-1}+1)I_{s,t-1}+\Phi^2_{s,2}\Phi_{s,1}(Age_{p,t-2}+2)I_{s,t-2}+\Phi_{s,3}Age_{f,t}Q_{f,t}+$ $\Phi_{s,2}\Phi_{s,3}(Age_{f,t-1}+1)Q_{f,t-1} + \Phi^2_{s,2}\Phi_{s,3}(Age_{f,t-2}+2)Q_{f,t-2})-$ $\Phi_{f,1}(Age_{f,t-1}+1)ET_{f,t}\}/(Q_{f,t}-\Phi_{f,3}\Phi_{s,3}Q_{s,t-2})$	

730

Table A2 Description of the calibrated parameters

Coefficient	Units	Descriptions
K_s	hour	The slow flow reservoir constant
K_f	hour	The fast flow reservoir constant
K_e	hour	Exchange constant between the two reservoirs
f	-	The ratio of porosity of the quick to slow flow reservoir
a	-	Precipitation recharge coefficient for slow flow reservoir
w	-	The hillslope unit constant
b	-	Recharge coefficient of Hillslope to slow flow reservoir
Is	-	Coefficient for evaporation fractionation
KK	-	Constant for calculation of rainfall recharging the active store in
pp	-	hillslope
con	-	Coefficient for exchange flow between active and passive stores in hillslope
fei	-	Weighting constant